

# Analyst

Accepted Manuscript



This is an *Accepted Manuscript*, which has been through the Royal Society of Chemistry peer review process and has been accepted for publication.

*Accepted Manuscripts* are published online shortly after acceptance, before technical editing, formatting and proof reading. Using this free service, authors can make their results available to the community, in citable form, before we publish the edited article. We will replace this *Accepted Manuscript* with the edited and formatted *Advance Article* as soon as it is available.

You can find more information about *Accepted Manuscripts* in the [Information for Authors](#).

Please note that technical editing may introduce minor changes to the text and/or graphics, which may alter content. The journal's standard [Terms & Conditions](#) and the [Ethical guidelines](#) still apply. In no event shall the Royal Society of Chemistry be held responsible for any errors or omissions in this *Accepted Manuscript* or any consequences arising from the use of any information it contains.

1  
2  
3  
4 **Fourier Transform Infrared Spectroscopy to Quantify Collagen**  
5 **and Elastin in an In Vitro Model of Extracellular Matrix**  
6  
7  
8 **Degradation in Aorta**  
9

10  
11 Rabee Cheheltani<sup>a</sup>, Cushla M. McGoverin<sup>b</sup>, Jayashree Rao<sup>c</sup>, David A. Vorp<sup>cd</sup>,  
12  
13 Mohammad F. Kiani<sup>ae</sup>, N. Pleshko<sup>b</sup>  
14  
15

16  
17  
18  
19 <sup>a</sup>*Department of Mechanical Engineering, Temple University, Philadelphia, PA 19122, USA*  
20

21 <sup>b</sup>*Department of Bioengineering, Temple University, Philadelphia, PA 19122, USA*  
22

23  
24 <sup>c</sup>*Department of Bioengineering, University of Pittsburgh, Pittsburgh, PA 15219 USA*  
25

26 <sup>d</sup>*Department of Cardiothoracic Surgery, and Surgery; the Center for Vascular Remodeling and*  
27 *Regeneration, and the Clinical and Translational Sciences Institute, University of Pittsburgh,*  
28 *Pittsburgh, PA 15219 USA*  
29

30 <sup>e</sup>*Department of Radiation Oncology, Temple University School of Medicine, Philadelphia, PA*  
31 *19140*  
32  
33  
34  
35  
36  
37  
38  
39  
40  
41  
42  
43  
44  
45  
46  
47  
48  
49  
50  
51  
52  
53  
54  
55  
56  
57  
58  
59  
60

## Abstract

Extracellular matrix (ECM) is a key component and regulator of many biological tissues including aorta. Several aortic pathologies are associated with significant changes in the composition of the matrix, especially in the content, quality and type of aortic structural proteins, collagen and elastin. The purpose of this study was to develop an infrared spectroscopic methodology that is comparable to biochemical assays to quantify collagen and elastin in aorta. Enzymatically degraded porcine aorta samples were used as a model of ECM degradation in abdominal aortic aneurysm (AAA). After enzymatic treatment, Fourier transform infrared (FTIR) spectra of the aortic tissue were acquired by an infrared fiber optic probe (IFOP) and FTIR imaging spectroscopy (FT-IRIS). Collagen and elastin content were quantified biochemically and partial least squares (PLS) models were developed to predict collagen and elastin content in aorta based on FTIR spectra. PLS models developed from FT-IRIS spectra were able to predict elastin and collagen content of the samples with strong correlations (RMSE of validation = 8.4% and 11.1% of the range respectively), and IFOP spectra were successfully used to predict elastin content (RMSE = 11.3% of the range). The PLS regression coefficients from the FT-IRIS models were used to map collagen and elastin in tissue sections of degraded porcine aortic tissue as well as a human AAA biopsy tissue, creating a similar map of each component compared to histology. These results support further application of FTIR spectroscopic techniques for evaluation of AAA tissues.

## Introduction

The aorta is the major blood vessel for transport of oxygenated blood from the heart to the arteries of the systemic circulation, and aortic diseases are among the leading causes of death in developed countries. The aorta is composed of three distinct structural layers or tunicae: the intima, media and adventitia, and the cellular and extracellular composition of these layers are related to their function<sup>1-3</sup>. The innermost layer, tunica intima, is essentially composed of a single layer of endothelial cells that are in direct contact with blood. The tunica media is composed of smooth muscle cells surrounded by an elastic extracellular matrix (ECM) of fibrous proteins, elastin and collagen. Elastin fibers provide the elastic properties and tensile strength of the aorta necessary for propulsion of the blood downstream. These fibers are arranged in concentric plates called elastic lamellae with a network of finer elastic fibers between lamellae. Collagen fibers, which are dispersed in the space between the lamellae, contribute to the strength and structural integrity of the aorta. The outermost layer of the aorta, tunica adventitia, is surrounded by loose connective tissue and mostly consists of bundles of thick collagen fibrils. In aging and disease, the fibrous structure and content of collagen and elastin in the aortic ECM change<sup>4-7</sup>. There is a direct relationship between the structural integrity of the compositional proteins and the healthy functionality of the aorta<sup>8,9</sup>. Therefore, characterization of the molecular changes in ECM has a critical role in the diagnosis and severity assessment of different pathological conditions. Moreover, such characterization provides useful information for deeper understanding of the pathophysiological mechanisms that underlie disease onset and progression.

One of the common diseases of the aorta is the focal dilatation of the infrarenal aorta known as abdominal aortic aneurysm (AAA). AAA, predominantly found in men 65 years of age and older, is associated with progressive destruction of the ECM structure and its major constituents, collagen and elastin macromolecules<sup>10,11</sup>, leading to wall weakening and dilatation<sup>12,13</sup>. Left untreated, the gradual expansion of the aorta and weakness of the vessel wall may lead to rupture and consequent death<sup>14</sup>. In current clinical practice, the necessity for surgical intervention to prevent rupture is determined by the maximum diameter of the aneurysm. However, several studies have found biomechanical properties to be more reliable predictors of rupture risk<sup>13-16</sup>. Since there is

1  
2  
3 a direct relationship between the level of ECM protein integrity and mechanical  
4 properties of the aorta<sup>9,17,18</sup>, a methodology that provides detailed knowledge of the  
5 molecular composition and content of the aortic wall in AAA patients would be extremely  
6 beneficial for precise diagnosis and rupture risk assessment. In this study, we introduce a  
7 novel application of Fourier transform infrared (FTIR) spectroscopy for the quantification  
8 of collagen and elastin in aorta.  
9

10  
11  
12  
13  
14 Recent infrared microscopy and imaging studies of cardiovascular tissues include  
15 monitoring arterial remodeling after injury<sup>19</sup>, identification and characterization of  
16 vulnerable plaques using characteristic absorption bands of lipids and total protein<sup>20–23</sup>,  
17 study of collagen deposition in cardiomyopathic heart sections<sup>24–26</sup> and assessment of  
18 cardiac remodeling after myocardial infarction<sup>27</sup>. In our laboratory, we have developed  
19 FTIR methodology to map collagen deposition in heart sections that had undergone  
20 cardiac remodeling after myocardial infarction<sup>28</sup>. In addition, FTIR has been used to  
21 characterize aneurysmal tissue in biopsies of human ascending aortas<sup>29–32</sup>. These  
22 investigators demonstrated that normal and aneurysmal human arterial tissue biopsies  
23 could be differentiated using the ratio of  $\alpha$ -helical to  $\beta$ -sheet structures and principal  
24 component analysis (PCA)<sup>29</sup>, hierarchical cluster analysis (HCA)<sup>30</sup> and factorial  
25 discriminant analysis (FDA)<sup>32</sup>. Furthermore, curve-fitting was applied to the spectra to  
26 detect alteration of  $\beta$  structures in the protein spectral profile of pathological aortas<sup>31</sup>.  
27 Although this group of studies set the ground work for differentiation of aneurysmal from  
28 healthy aortic tissues, there has been minimal confirmation with histology or biochemical  
29 analysis, and the relative degradation of the primary ECM components (elastin and  
30 collagen) associated with aneurysm condition has not been specifically evaluated.  
31

32  
33  
34  
35  
36  
37  
38  
39  
40  
41  
42  
43  
44 In this study, we develop multivariate regression models to quantify collagen and  
45 elastin in degraded aorta, using FTIR spectroscopic methods. We hypothesize that our  
46 methodology is comparable to biochemical measurements for quantifying collagen and  
47 elastin and present a systematic comparison of these two techniques. The motivation for  
48 development of this methodology is twofold: first, FTIR has the potential of translation to  
49 a clinical diagnostic method through the use of infrared fiber optic probe (IFOP)  
50 technology<sup>33–35</sup>. For cardiovascular tissues specifically, the potential of catheter based  
51 IFOPs for the characterization of atherosclerotic plaques has gained increasing  
52  
53  
54  
55  
56  
57  
58  
59  
60

1  
2  
3 attention<sup>36-38</sup>. As a second motivation, a better understanding of the pathophysiology of  
4 AAA is dependent on development of methods that can reliably measure content and  
5 distribution of various ECM components. Fourier transform infrared imaging  
6 spectroscopy (FT-IRIS) has been increasingly used to create chemical images of various  
7 components in biological tissue<sup>20,28,32,39</sup>. Here, we have used these two modalities of FTIR  
8 analysis, IFOP on intact tissues, and FT-IRIS on histological tissue sections, to quantify  
9 collagen and elastin in proteolytically treated aorta samples as a model of AAA disease<sup>9</sup>.  
10 FTIR spectra collected from each modality were correlated to elastin or collagen content  
11 in multivariate models applying the partial least squares (PLS) regression method. To  
12 demonstrate an application of the developed methodology, the FT-IRIS based PLS  
13 regression models were applied to aortic histological sections, resulting in a map of ECM  
14 components in these tissue sections. It should be emphasized that despite being presented  
15 in the context of AAA disease, this methodology is applicable to any aortic pathological  
16 condition that is identified with a change in the content of collagen or elastin in aortic  
17 ECM.  
18  
19  
20  
21  
22  
23  
24  
25  
26  
27  
28  
29  
30

## 31 **Materials and Methods**

### 32 **Preparation of the aorta samples**

33  
34  
35 Two porcine aortas were purchased from a local slaughterhouse and transferred on ice  
36 before being cut into rings of about 2-3 cm in length (Fig 1-A). These aorta rings were  
37 embedded in optimal cutting temperature (OCT) compound (Tissue Tek, Sakura Finetek,  
38 Torrance, CA) to preserve the structure, flash frozen and kept at -80°C before being cut  
39 into samples for enzymatic degradation as explained below.  
40  
41  
42  
43  
44  
45

46 (Fig. 1 here)

47 **Figure 1** Experimental procedure. A) Porcine descending aorta cut in 2-3 cm long rings.  
48 B) Aorta rings cut open and cut in smaller pieces for enzymatic degradation. C) Custom  
49 ATR sampling tip for FTIR-IFOP data collection next to an American quarter dollar coin.  
50 D) FTIR-IFOP data collection from an aorta sample.  
51  
52  
53  
54  
55  
56  
57  
58  
59  
60

### Enzymatic degradation of the aorta samples

Frozen aorta rings selected from different anatomical locations along the aorta were thawed in PBS at 37°C, and their OCT dissolved by washing the samples in deionized (DI) water. Aorta rings were then cut into circumferential strip samples of *ca.* 100 mg wet tissue weight (Fig 1-B). Samples were then treated with collagenase, elastase or buffer (untreated) for 2, 5 or 24 hours for a total of 9 treatment groups. Collagenase treatment was applied by leaving the sample submerged in 500 ml of collagenase solution for the specified treatment time at 37°C. Collagenase solution was prepared by dissolving purified collagenase (CLSPA, Worthington Biochemical, Lakewood, NJ) in tris-buffered saline (TBS, pH 8.0) at a concentration of 1 mg/ml. Elastase treated samples were left in 500 ml of elastase solution for the specified treatment time at room temperature. Elastase solution was prepared by dissolving purified elastase (ESFF, Worthington Biochemical, Lakewood, NJ) in TBS (0.5 mg/ml). Untreated samples were left in 500 ml of TBS at room temperature. A total of 81 samples were prepared. After the specified treatment time, samples were washed with DI water and FTIR-IFOP data were collected as detailed below. Each sample was then cut in half along the aorta circumference. One half was put in OCT compound, flash frozen and stored at -80°C for further histologic sectioning. The remaining half was weighed (wet weight), minced into smaller tissue pieces, and lyophilized for use in biochemical assays of elastin and collagen content. Biochemically measured elastin and collagen content were expressed as either mass percentage of wet tissue (%ww) or mass percentage of dry matter after lyophilization (%dw).

### Biochemical analysis for quantification of elastin and collagen

Minced lyophilized samples were divided into two groups for the two biochemical assays. In the first group, elastin in the samples was converted to soluble cross-linked polypeptide elastin fragments, known as  $\alpha$ -elastin<sup>40</sup>, by 0.25 M oxalic acid extraction at 100°C. A total of four 1 hour extractions were necessary to completely dissolve the elastin in the aorta samples. The amount of  $\alpha$ -elastin in the resulting solutions was measured using Fastin Elastin Assay (Biocolor, Carrickfergus, UK) according to the manufacturer instructions. For collagen quantification, the hydroxyproline content of the other group of the lyophilized samples was measured by oxidation with sodium peroxide and the formation

1  
2  
3 of an intense red color with p-dimethylaminobenzaldehyde (DMAB)<sup>41</sup>. Collagen content  
4 in the samples was estimated by assuming 12.5g hydroxyproline/100g collagen<sup>42</sup> after  
5 correction for hydroxyproline content in elastin (1.5g hydroxyproline/100g elastin<sup>42-44</sup>).  
6  
7  
8

### 9 **FTIR Fiber optic probe (IFOP) data collection**

10  
11 IFOP spectra were collected with a custom-made silver halide attenuated total reflectance  
12 (ATR) sampling tip (Art Photonics, Berlin, Germany). The tip was mounted to the end of  
13 a 1 m silver halide fiber, which was connected to a Fibermate 2 fiber-optic probe launcher  
14 (Harrick Scientific Products, Pleasantville, NY). The launcher was coupled to a Nicolet  
15 iS5 spectrometer (Thermo Scientific, Madison, WI). The custom-made ATR sampling tip  
16 was 15 cm in length and had a diameter of 3 mm (Fig 1-C). Freshly treated samples were  
17 washed in DI water and excess water was removed before data collection. IFOP spectra  
18 were collected from 3 points on the intima and 3 points on the adventitia side of the  
19 sample. The sampling tip was held by hand in contact with the sample (Fig 1-D).  
20 Background spectra were collected by holding the sampling tip in the air. Each spectrum  
21 was collected in the range 750-4000 cm<sup>-1</sup> with 64 co-added scans and a spectral resolution  
22 of 8 cm<sup>-1</sup>.  
23  
24  
25  
26  
27  
28  
29  
30  
31  
32

### 33 **FT-IRIS data collection and analysis**

34  
35 Enzymatically degraded frozen aorta samples were cryosectioned (9 μm-thick aortic cross  
36 section), mounted on MirrIR low-e microscope slides (Kevley Technologies, Chesterland,  
37 OH). OCT on the slide was washed off carefully with DI water and samples were fixed in  
38 10% formalin for 10 minutes to maintain the morphology. FT-IRIS images were acquired  
39 at 50 μm pixel resolution and 8 cm<sup>-1</sup> spectral resolution with 2 co-added scans using a  
40 Perkin Elmer Spotlight 400 spectrometer (Shelton, CT) in transflection mode.  
41 Background spectra for each sample were collected from a region on the slide with no  
42 tissue. FT-IRIS data were analyzed in ISys 5.0 software (Malvern Instruments Ltd,  
43 Malvern, UK). For each sample, the average spectrum of all pixels in the image was  
44 calculated and used in PLS models to predict elastin and collagen dry weight content.  
45  
46  
47  
48  
49  
50  
51  
52  
53  
54  
55  
56  
57  
58  
59  
60

## PLS models

PLS analysis and spectral preprocessing were performed in The Unscrambler X software (CAMO Software AS, Oslo, Norway). A total of four PLS models were created (summarized in Table 1). ELAS and COL models refer to models for elastin content and collagen content respectively.

(Table 1 here)

**Table 1** Summary of the PLS models and their abbreviations in this article

Model abbreviation	Component	Model of spectral collection	Reference content	Assay for reference content measurement
COL-IFOP	Collagen	Infrared fiber optic probe (IFOP)	mass percentage in wet tissue (%ww)	Hydroxyproline assay
ELAS-IFOP	Elastin	Infrared fiber optic probe (IFOP)	mass percentage in wet tissue (%ww)	Fastin elastin assay
COL-FTIRIS	Collagen	Infrared imaging spectroscopy (FT-IRIS)	mass percentage in dry matter (%dw)	Hydroxyproline assay
ELAS-FTIRIS	Elastin	Infrared imaging spectroscopy (FT-IRIS)	mass percentage in dry matter (%dw)	Fastin elastin assay

Two PLS models were created for collagen and elastin content prediction using IFOP spectra. The six spectra collected per sample (three from the intima side and three from the adventitia side) were averaged prior to spectral preprocessing. Averaging of the spectra was performed to be commensurate with comparisons to collagen and elastin content from biochemical analysis obtained from samples that contained all layers. Spectral bands attributed to elastin and collagen were apparent between 1000 and 1800  $\text{cm}^{-1}$ ; this spectral region was subsequently used for analysis. An extended multiplicative scatter correction (EMSC)<sup>45,46</sup> was applied to the spectra, followed by calculation of the second derivative of the spectra (third order polynomial and 11 smoothing points). Samples were divided into two independent calibration and validation sets. Two thirds of

1  
2  
3 the samples (54 samples for ELAS model and 48 samples for COL model) were assigned  
4 to the calibration set and were correlated with reference content (%ww) of collagen  
5 (COL-IFOP model) or elastin (ELAS-IFOP model) measured previously by biochemical  
6 assays. The average spectra of the remaining samples (27 samples for ELAS model and  
7 24 samples for COL model) were used as the validation set<sup>47-49</sup>. For these sets to be  
8 representative of the whole range of the measured values for samples, they were carefully  
9 assigned such that both included samples from all treatment groups and samples from  
10 different anatomical positions of the aorta.  
11

12  
13  
14  
15  
16  
17  
18 Two PLS models for collagen and elastin content were developed based on FT-IRIS  
19 spectra of sections from enzymatically degraded aorta specimens mounted on low-e  
20 slides. Average spectra per image for each specimen were used in the models and similar  
21 pre-processing methods as used for the IFOP models were applied. The second derivative  
22 was calculated with a third order polynomial and 9 smoothing points. The same  
23 calibration and validation sets as used in PLS-IFOP models were used and FT-IRIS  
24 spectra were correlated with reference content (%dw) of collagen (COL-FTIRIS model)  
25 or elastin (ELAS-FTIRIS model) measured previously by biochemical assays.  
26  
27  
28  
29  
30  
31

### 32 **Pure component pellets**

33  
34 Potassium bromide pellets were prepared using pure powders of collagen (primarily type  
35 I) from bovine achilles tendon (C206, Elastin Products Company, Owensville, MO) and  
36 porcine aortic elastin (SP46, Elastin Products Company, Owensville, MO). The purchased  
37 collagen was in the form of shredded fibers and was milled into fine powder using a  
38 cryogenic mill (6770 Freezer/Mill, SPEX Sample Prep, Metuchen, NJ). Pellets were  
39 prepared by mixing 4 mg of component powder with 196 mg of KBr and compressing the  
40 mixture into a pellet. The 4 mg component powder was prepared from a mixture of  
41 elastin/collagen powders in 0/100, 50/50, 100/0 percentages by weight (n=6 for each  
42 percentage). FTIR Spectra were acquired at 2 cm<sup>-1</sup> spectral resolution with 64 co-added  
43 scans using the Perkin Elmer Spotlight 400 spectrometer. Spectra presented for each  
44 group were calculated by averaging the spectra of six pellets within each group.  
45  
46  
47  
48  
49  
50  
51  
52  
53  
54  
55  
56  
57  
58  
59  
60

### Mapping components in aorta sections and human AAA section

A 5 hour elastase treated sample and a 5 hour collagenase treated sample were selected and consecutive 9  $\mu\text{m}$ -thick sections were obtained by cryosectioning and mounted on to MirrIR low-e microscope slides and glass slides for FT-IRIS and histology respectively. Sections of a human AAA wall specimen were prepared similarly. This specimen was obtained from an AAA patient during elective surgical repair (obtained under University of Pittsburgh IRB approval), paraffin embedded, and sectioned onto MirrIR low-e and glass slides. The section on low-e slide was deparaffinized by heating the slide at 60°C for two hours followed by an immersion in Xylenes and subsequent hydration of the tissue with decreasing grades of alcohol. After deparaffinization, FT-IRIS images were collected at 6.25  $\mu\text{m}$  pixel resolution and 8  $\text{cm}^{-1}$  spectral resolution, with 2 co-added scans per pixel. Second derivative of the spectra in the images were calculated with third order polynomial and 9 smoothing points similar to PLS-FTIRIS models mentioned above. Spectra were vector normalized and exported to MATLAB R2013a (Mathworks, Inc., Natick, MA). Regression coefficients of COL-FTIRIS and ELAS-FTIRIS PLS models were also imported and used to predict collagen and elastin content respectively for each image pixel. Maps of elastin or collagen content in the sections were created by the scalar product of each pixel spectrum and the regression coefficients.

### Histological staining

The histology sections from the 5 hour elastase treated specimen was stained using the Verhoeff-Van Gieson (VVG) Staining Protocol for Elastic Fibers stain kit (Polysciences Inc., Warrington, PA). The 5 hour collagenase treated specimen sections were stained with picosirius red stain kit (Polysciences Inc., Warrington, PA). The AAA wall section was being used in another study and was stained with Movat's pentachrome staining protocol. Histology images were acquired using a Nikon microscope equipped with a Nikon DS-Fi1 color camera and Nikon Element software (Nikon Instruments Inc., Mellville, NY). Images of collagen distribution in the picosirius red stained sections, were obtained under linearly polarized light as detailed previously<sup>50</sup>.

## Results and Discussion

### Measured collagen and elastin content in aorta Using Biochemical Assays

The overall elastin and collagen contents of untreated samples (n=27), and the variation of collagen and elastin content in samples from upper thoracic (n=9) and lower thoracic (n=9), were in agreement with previous studies<sup>43,44</sup>. Average elastin content in different untreated aortic rings ranged from 45% ( $\pm 4\%$ ) to 59% ( $\pm 5\%$ ) (%dw). Samples from anatomical positions closer to the arch (upper thoracic) on average had higher values than those closer to abdominal section (lower thoracic) (Fig 2-A). The gradual decrease of elastin proportion in descending aorta from arch to abdominal has been reported in several mammals and has been associated with less elasticity needed in distal regions as the blood flows further from the heart<sup>51</sup>. Collagen proportion in different untreated aortic rings ranged from 4.1% ( $\pm 0.1\%$ ) to 20% ( $\pm 1\%$ ) (%dw). Collagen content was lower in the samples from upper thoracic regions of the aorta and higher in samples from lower thoracic regions (Fig 2-B).

(Fig. 2 here)

**Figure 2** Elastin and collagen content in porcine descending aorta in different anatomical locations (n=9 per group, error bars are standard error of the mean). A) Elastin content in the descending aorta decreases from upper to lower aorta (P=0.002). B) Collagen content in the descending aorta increases from upper to lower aorta (P=0.014).

In treated samples, elastin was lowest in samples treated with elastase for 24 hours (zero or close to zero) and highest in samples treated with collagenase for 24 hours. Collagen content was conversely highest in elastase treated samples and lowest in collagenase treated samples. Since treatment with elastase for 24 hours resulted in almost complete degradation of elastin, samples within this treatment group lost about half of their dry matter weight. In these samples, the remaining mass after treatment was too low for two biochemical assays, and priority was given to elastin assay. As a result, these samples were not included in the PLS models for collagen content. The most prominent feature of ECM changes in AAA is a wide scale depletion of elastin<sup>51,52</sup> and our elastase

1  
2  
3 treated samples provide a good model for AAA disease condition in terms of elastin  
4 degradation.  
5  
6

### 7 **FTIR Spectral Features of Elastin, Collagen and Aorta Samples**

8  
9  
10 The spectra of collagen and elastin show several similarities as seen in the KBr pellet  
11 spectra (Fig. 3-A and 3-B). They both have features that arise from their protein structure,  
12 including amide I (approximately 1580-1718  $\text{cm}^{-1}$ ) and amide II (approximately 1480-  
13 1580  $\text{cm}^{-1}$ ) absorbances. More interesting was the observation that the peak at 1338  $\text{cm}^{-1}$ ,  
14 which we have previously shown to be a strong quantifying peak for collagen scar  
15 deposition in infarcted cardiac tissue sections<sup>28</sup>, had a very similar absorbance in the  
16 collagen and elastin spectra. This band has been assigned to the  $\text{CH}_2$  wagging vibration of  
17 proline side chains<sup>53</sup>, and the similar absorbance of this band in collagen and elastin could  
18 be originating from the similar proline content of collagen and elastin (119 and 115  
19 residues in 1000 residues respectively<sup>42-44</sup>).  
20  
21  
22  
23  
24  
25  
26  
27  
28

29 (Fig. 3 here)

30  
31 **Figure 3** Average spectra of samples with low, medium and high elastin content. A)  
32 Reference spectra of collagen-elastin KBr pellets, and B) second derivative of (A). C)  
33 FT-IRIS spectra, D) second derivative of (C), E) FTIR-IFOP spectra, and F) second  
34 derivative of (E). Samples in C and D were categorized into Low (0-26 %dw), Medium  
35 (27-52 %dw) and High (52-78 %dw) and samples in E and F were categorized into Low  
36 (0-5 %ww), Medium (8-14 %ww) and High (14-21 %ww) elastin content as measured by  
37 Fastin elastin assay. The numerical values for the spectra in this figure can be accessed as  
38 supplementary material.  
39  
40  
41  
42  
43  
44  
45

46  
47 Despite the similarities, collagen and elastin had some distinct differences, such as the  
48 spectral features in the 1040-1100  $\text{cm}^{-1}$  and 1380-1420  $\text{cm}^{-1}$  regions. As expected, the  
49 spectra of aorta (Fig. 3-C to 3-F) and the spectra of its major constituents, collagen-elastin  
50 mixture (Fig. 3-A and 3-B), are similar in general features such as the prominent peaks of  
51 amide I and amide II bands. These spectral bands appear broader in KBr pellets due to  
52 scattering effects. Differences between collagen-elastin mixture spectra and aorta spectra  
53  
54  
55  
56  
57  
58  
59  
60

1  
2  
3 are attributed to other minor aorta constituents, e.g. proteoglycan and glycoproteins of the  
4  
5 ECM and actin and myosin proteins of the smooth muscle cells.  
6

7 To study the effects of elastin degradation in FTIR spectra, samples were divided into  
8  
9 groups of low, medium and high elastin content as measured from Fastin elastin assay. To  
10 study FT-IRIS features (Fig. 3C and 3D), samples were categorized according to their  
11 %dw elastin content into Low (0.0-26 %dw), Medium (27-51 %dw) and High (52 -78  
12 %dw). To study IFOP spectral features (Fig. 3E and 3F), samples were categorized newly  
13 according to their %ww elastin content into Low (0-5 %ww) Medium (8-14 %ww) and  
14 High (14-21 %ww). It should be noted that these categorizations were merely based on  
15 final measurement of elastin content in the samples, and this variation was due to both  
16 anatomical location and enzymatic degradation. Characterization of the separate effects  
17 caused by each of these parameters in elastin content of each sample was out of the scope  
18 of this study.  
19

20 One of the most prominent spectral features of decreasing elastin content in aorta is the  
21 shift in amide II peak toward higher wavenumbers (Figures 3-C and 3-E). This could be  
22 explained by differences in amino acid compositions of collagen and elastin. For  
23 example, collagen has 9.5% glutamine<sup>54</sup>, whereas elastin has 1.7% glutamine<sup>55</sup> and  
24 glutamine has vibrational peaks at 1556-1560 cm<sup>-1</sup><sup>56</sup>. The shift in amide II towards higher  
25 vibrational peaks can be tentatively assigned to a depleted spectral contribution from  
26 glutamine.  
27

28 The underlying features of the amide I band were resolved by examining second  
29 derivative spectra. Two peaks were observed in the amide I region of FT-IRIS and KBr  
30 pellet spectra. The peak at approximately 1630 cm<sup>-1</sup> slightly shifted to higher  
31 wavenumbers with decreasing elastin content (Fig. 3-B,D). This slight shift may be  
32 explained by the differences in secondary structures of collagen and elastin<sup>29,31,57</sup>.  
33 Collagen is composed mainly of  $\alpha$ -helical structures, while elastin is primarily  $\beta$ -sheets;  
34 the amide I band of  $\alpha$ -helical structures occurs between 1643-1667 cm<sup>-1</sup>, and for  $\beta$ -sheet  
35 structures occurs between 1610-1645 cm<sup>-1</sup><sup>29,57</sup>.  
36

37 There is a noticeable difference in the amide I/amide II intensity ratio between IFOP  
38 and FT-IRIS spectra, which can be attributed to the contribution of O-H bending vibration  
39 of water at 1640 cm<sup>-1</sup><sup>53</sup>. IFOP spectra were collected from freshly treated tissues  
40  
41  
42  
43  
44  
45  
46  
47  
48  
49  
50  
51  
52  
53  
54  
55  
56  
57  
58  
59  
60

1  
2  
3 containing water, whereas FT-IRIS spectra were collected from dehydrated tissue  
4 sections. There is also an increase in intensity of amide I with lower elastin content seen  
5 in FT-IRIS (Fig. 3-C) and pellet spectra (Fig. 3-A) which is not noticeable in IFOP  
6 spectra (Fig 3-E). This may be due to the fact that samples with low elastin content, i.e.  
7 samples treated with elastase for longer treatment times, would lose their original solid  
8 structure and absorb water 3-4 times their original water content. This inverse relationship  
9 between elastin and water content in the elastase treated samples may have resulted in  
10 higher absorbance from higher water content balancing the effect of elastin loss in amide  
11 I region in these samples. In addition, IFOP spectra were inherently different from spectra  
12 collected using the FT-IRIS imaging system. IFOP spectra were collected using an ATR  
13 technique; in ATR, infrared light is shone onto a sample through a high refractive index  
14 material, most of the light is totally internally reflected however a small amount of light  
15 penetrates into the sample, this is known as an evanescent wave. An ATR spectrum is  
16 based on the absorption profile of this evanescent wave and because of the depth  
17 penetration characteristics of this evanescent wave ATR spectra are different to those  
18 collected using the FT-IRIS imaging system. The depth of penetration of the evanescent  
19 wave is dependent on both wavelength and the refractive index of the sample such that  
20 penetration depth, and therefore effective pathlength, is greatest at longer wavelengths.  
21 This greater effective pathlength results in an enhancement of absorption features at  
22 longer wavelengths<sup>58</sup>. ATR correction algorithms can be used in many ATR applications  
23 with crystal based ATR tips where the pathlength of the evanescent wave is known.  
24 However, in this study, due to the complicated loop-shaped geometry of the custom-made  
25 ATR tip (Fig 1-C) and the unknown pathlength of the wave, ATR correction could not be  
26 applied.  
27  
28  
29  
30  
31  
32  
33  
34  
35  
36  
37  
38  
39  
40  
41  
42  
43  
44  
45

### 46 PLS Models

47  
48 The results for PLS regression models are presented in Figure 4. As the plots show, in all  
49 models both calibration and validation sets span the whole range of the samples under  
50 study. The developed PLS models strongly correlated with measured numbers, with the  
51  $R^2$  for regression lines exceeding 0.7 for all but the COL-IFOP model. More importantly,  
52 the error of prediction of the three strongest models was ~10% of the range of  
53 measurements. These results confirm that elastin and collagen concentration can be  
54  
55  
56  
57  
58  
59  
60

1  
2  
3 predicted in aorta samples using infrared imaging spectroscopy of their histology  
4 sections. Furthermore, elastin concentration can be estimated using infrared fiber optic  
5 probe spectra taken from bulk tissue samples.  
6  
7  
8  
9

10  
11 (Fig. 4 here)

12 **Figure 4** Spectroscopically predicted vs. biochemically measured reference values for the  
13 developed PLS models as detailed in Table 1. Calibration set is marked in blue and  
14 validation set is marked in red. The number of factors in Y axis titles are the number of  
15 factors used to build the PLS model.  
16  
17  
18  
19

20  
21 In general, the models predicting elastin were more accurate than collagen models.  
22 Elastin is the major ECM component in aorta with quantities more than twice the amount  
23 of collagen quantity. Therefore, the greater contribution of elastin to the mid-infrared  
24 spectra means that variations in elastin content will be more obvious spectrally. In  
25 addition, the measurement error associated with collagen content was greater than elastin  
26 content. We estimated the collagen content in our samples by determining hydroxyproline  
27 concentration, which is a very well established method for estimating collagen content in  
28 biological tissues<sup>41,42,44,59</sup>. Because of the low hydroxyproline content of elastin, the  
29 contribution of elastin to total hydroxyproline is neglected in most applications of this  
30 method. However, in our study we applied enzymes to degrade collagen and elastin to  
31 varying degrees, and because of the varying ratio of elastin to collagen content in our  
32 samples we could not neglect the contribution of elastin to hydroxyproline concentration.  
33 For this reason, collagen was calculated from the hydroxyproline assay after the  
34 contribution from elastin was accounted for. While this approach would assure more  
35 realistic values for collagen content, the errors in the elastin assay were introduced into  
36 the estimation of collagen and add to intrinsic errors in the hydroxyproline assay. This  
37 could also explain a number of negative collagen values which were observed in samples  
38 treated with 24 hours collagenase. These samples were expected to have close to zero  
39 collagen content as confirmed with histology (data not shown), and the negative values  
40 could have resulted from the assumed hydroxyproline content in elastin (1.5%) being an  
41 overestimation.  
42  
43  
44  
45  
46  
47  
48  
49  
50  
51  
52  
53  
54  
55  
56  
57  
58  
59  
60

1  
2  
3  
4  
5  
6  
7  
8  
9  
10  
11  
12  
13  
14  
15  
16  
17  
18  
19  
20  
21  
22  
23  
24  
25  
26  
27  
28  
29  
30  
31  
32  
33  
34  
35  
36  
37  
38  
39  
40  
41  
42  
43  
44  
45  
46  
47  
48  
49  
50  
51  
52  
53  
54  
55  
56  
57  
58  
59  
60

The higher signal to noise ratio of FT-IRIS spectra vs. IFOP spectra may also contribute to FT-IRIS models being stronger than IFOP models. IFOP spectra were collected and averaged from six points on the surface of the sample whereas FT-IRIS spectra were averaged from the pixels in the hyper-spectral images of the aortic wall cross section which were *ca.* 3500-9000 pixels for each sample. Furthermore, the proteolytically degraded samples were heterogeneous as the enzyme treatments degraded the aorta samples from the outer surfaces. This effect can be seen by comparing images of untreated samples (Fig. 5-A and 5-B) to samples treated with elastase and collagenase for 5 hours (Fig. 5-C and 5-D respectively). In the elastase treated sample (Fig. 5-C) elastic lamellae, as differentiated in black in the Verhoeff Van Geisen staining, was degraded completely in the peripheries, with the core still packed with elastic lamellae. In Figure 5-D, the same pattern exists with collagen fibers visualized as bright yellow in the picrosirius red stain under polarized light. This spatial variation of components in the partially degraded samples could have resulted in sampling errors in collecting the spectra using the IFOP from the surface of the sample. Finally, contribution of water in the spectra could be another reason for a weaker correlation between content and spectra in IFOP models. IFOP spectra were collected from samples containing water, and in the case of elastase treated samples, additional water is likely to have been absorbed. Despite a lower sensitivity of IFOP spectral data collection compared to FT-IRIS, they each have distinct applications. IFOP data collection has the advantage that it is transferrable to a clinical environment with further development of the technology. Consideration of spectral interference from blood in our model could also improve its utility. FT-IRIS is an imaging technology which is useful in mapping components at high spatial resolution on histological sections as observed in the example application below.

(Fig. 5 here)

**Figure 5** Histological and FT-IRIS images of aorta samples. FT-IRIS images are intensity images in pseudo-color increasing in intensity from blue to red. A) Verhoeff-Van Gieson (VVG) staining of an untreated sample with elastin stained black. B) Polarized image of a picrosirius red staining of an untreated sample with collagen fibers visualized as bright yellow-orange. C) VVG staining of a sample treated with elastase for 5 hours. D) Polarized image of a picrosirius red

1  
2  
3 staining in a sample treated with collagenase for 5 hours. E) FT-IRIS mapping of elastin in a  
4 consecutive section from the sample in (C). F) FT-IRIS mapping of collagen in a consecutive  
5 section from the sample in (D). G) Movat's pentachrome staining of a section of a human AAA  
6 sample visualizing pathological aggregates of elastin fibers as black (area denoted with arrows),  
7 collagen as yellow-brown, proteoglycans in blue and fibrin in red. H) FT-IRIS mapping of  
8 elastin in the sample in (G). I) FT-IRIS mapping of collagen in the sample in (G).  
9  
10  
11  
12  
13  
14  
15

### 16 **Mapping components in aorta sections and human AAA section**

17  
18 To further validate the results of the FT-IRIS models, and to demonstrate their application  
19 for investigation of AAA disease, we used the results of these PLS models to create maps  
20 of elastin and collagen on histological sections of degraded aorta as well as sections from  
21 the aorta of a patient with an AAA.  
22  
23

24  
25 Figures 5-E and 5-F show the FT-IRIS mapping of elastin and collagen using the  
26 regression coefficient of the corresponding FT-IRIS PLS model as explained in the  
27 methods section. These images, similar to their corresponding histological sections (Fig.  
28 5-C and 5-D), show a complete degradation of elastin or collagen in the peripheries that  
29 were in direct contact with the enzyme.  
30  
31  
32  
33

34 The histopathological features of AAA pathology are noticeable in the Movat's  
35 pentachrome section shown in figure 5-G where the normal alignment of elastin and  
36 collagen fibers is absent. Instead of organized elastin lamella across the whole thickness  
37 of the section, elastin has aggregated in the triangular area pointed by the arrows, with the  
38 rest of the section completely depleted of elastin. The distribution of elastin determined  
39 using FT-IRIS and the ELAS-FTIRIS PLS model (Fig. 5-H) and the distribution of  
40 collagen using COL-FTIRIS model (Fig. 5-I) are comparable to Movat's pentachrome  
41 staining. The fact that the results of the PLS model based on enzymatically degraded  
42 swine aorta samples could be applied with this level of similarity to histology in this  
43 human AAA section, is a strong indication of the applicability of the developed models to  
44 human tissues.  
45  
46  
47  
48  
49  
50  
51  
52  
53  
54  
55  
56  
57  
58  
59  
60

## Conclusions

FTIR spectroscopy is a viable method for predicting collagen and elastin content in aortic tissue. We have created PLS models that can be applied to histological sections of the aortic tissue. This methodology to map collagen or elastin in aortic tissue is a useful tool in studying changes of ECM in different aortic diseases, with minimal preparation of the sections compared to histological or immunohistochemical methods. Also, a quantitative analysis of images would be fast and easy without complications attributed to image processing methods of histological images. We have also developed a PLS model to quantify elastin in “intact” aortic tissue using an infrared fiber optic probe. This methodology could prove useful when fiber optic technology advances to the point of being applicable in vivo for diagnosis or risk assessment of pathological conditions of the aorta including AAA.

## Acknowledgements

This work was supported by National Institutes of Health (NIH) grant number HL086418.

## References

1. T. C. Gasser, R. W. Ogden, and G. a Holzapfel, *J. R. Soc. Interface*, 2006, **3**, 15–35.
2. G. A. Antoniou, G. S. Georgiadis, S. A. Antoniou, F. A. Grandrath, A. D. Giannoukas, and M. K. Lazarides, *J. Vasc. Surg.*, 2011, **54**, 1175–81.
3. J. E. Wagenseil and R. P. Mecham, *Physiol. Rev.*, 2009, **89**, 957–989.
4. A. Tsamis, J. T. Krawiec, and D. A. Vorp, *J. R. Soc. Interface*, 2013, **10**, 20121004.
5. G. Vieira-Damiani, D. P. Ferro, R. L. Adam, A. A. de Thomaz, V. Pelegati, C. L. Cesar, and K. Metze, in *Multiphoton Microscopy in the Biomedical Sciences XI*, eds. A. Periasamy, K. König, and P. T. C. So, 2011, p. 79030B–79030B–8.
6. J. E. Wagenseil and R. P. Mecham, *J. Cardiovasc. Transl. Res.*, 2012, **5**, 264–73.
7. T. Toda, N. Tsuda, I. Nishimori, D. E. Leszczynski, and F. A. Rummerow, *Cells Tissues Organs*, 1980, **106**, 35–44.
8. J. H. N. Lindeman, B. A. Ashcroft, J.-W. M. Beenakker, M. van Es, N. B. R. Koekkoek, F. A. Prins, J. F. Tielemans, H. Abdul-Hussien, R. A. Bank, and T. H. Oosterkamp, *Proc. Natl. Acad. Sci. U. S. A.*, 2010, **107**, 862–5.
9. J. A. Kratzberg, P. J. Walker, E. Rikkers, and M. L. Raghavan, *J. Mech. Behav. Biomed. Mater.*, 2009, **2**, 65–72.
10. G. T. Jones, in *Diagnosis, Screening and Treatment of Abdominal, Thoracoabdominal and Thoracic Aortic Aneurysms*, ed. R. Grundmann, InTech, 2011, pp. 53–74.

11. F. A. M. V. I. Hellenthal, W. A. Buurman, W. K. W. H. Wodzig, and G. W. H. Schurink, *Nat. Rev. Cardiol.*, 2009, **6**, 464–74.
12. E. S. Di Martino, A. Bohra, J. P. Vande Geest, N. Gupta, M. S. Makaroun, and D. A. Vorp, *J. Vasc. Surg. Off. Publ. Soc. Vasc. Surg. [and] Int. Soc. Cardiovasc. Surgery, North Am. Chapter*, 2006, **43**, 570–6; discussion 576.
13. J. P. Vande Geest, E. S. Di Martino, A. Bohra, M. S. Makaroun, and D. a Vorp, *Ann. N. Y. Acad. Sci.*, 2006, **1085**, 11–21.
14. D. A. Vorp, *J. Biomech.*, 2007, **40**, 1887–902.
15. D. A. Vorp and J. P. Vande Geest, *Arterioscler. Thromb. Vasc. Biol.*, 2005, **25**, 1558–66.
16. J. Hua and W. R. Mower, *J. Vasc. Surg.*, 2001, **34**, 308–15.
17. E. Fonck, G. Prod'hom, S. Roy, L. Augsburg, D. A. Rüfenacht, and N. Stergiopoulos, *Am. J. Physiol. Heart Circ. Physiol.*, 2007, **292**, H2754–63.
18. M. F. Fillinger, S. P. Marra, M. L. Raghavan, and F. E. Kennedy, *J. Vasc. Surg.*, 2003, **37**, 724–32.
19. B. C. Herman, R. Kundi, D. Yamanouchi, K. C. Kent, B. Liu, and N. Pleshko, *Proc. SPIE*, 2009, **7182**, 7182H1–7182H–12.
20. C. S. Colley, S. G. Kazarian, P. D. Weinberg, and M. J. Lever, *Biopolymers*, 2004, **74**, 328–35.
21. S. G. Kazarian and K. L. A. Chan, *Biochim. Biophys. Acta*, 2006, **1758**, 858–67.
22. F. Palombo, S. G. Cremers, P. D. Weinberg, and S. G. Kazarian, *J. R. Soc. Interface*, 2009, **6**, 669–80.
23. F. Palombo, H. Shen, L. E. S. Benguigui, S. G. Kazarian, and R. K. Upmacis, *Analyst*, 2009, **134**, 1107–18.
24. P. S. Bromberg, K. M. Gough, and I. M. C. Dixon, *Can. J. Chem.*, 1999, **77**, 1843–1855.
25. K. M. Gough, D. Zelinski, R. Wiens, M. Rak, and I. M. C. Dixon, *Anal. Biochem.*, 2003, **316**, 232–42.
26. K. Z. Liu, I. M. Dixon, and H. H. Mantsch, *Cardiovasc. Pathol.*, 1999, **8**, 41–7.
27. K. Lui, M. Jackson, M. G. Sowa, H. Ju, I. M. Dixon, and H. H. Mantsch, *Biochim. Biophys. Acta*, 1996, **1315**, 73–7.
28. R. Cheheltani, J. M. Rosano, B. Wang, A. K. Sabri, N. Pleshko, and M. F. Kiani, *J. Biomed. Opt.*, 2012, **17**, 056014.
29. F. Bonnier, S. Rubin, L. Ventéo, C. M. Krishna, M. Pluot, B. Baehrel, M. Manfait, and G. D. Sockalingum, *Biochim. Biophys. Acta*, 2006, **1758**, 968–73.
30. S. Rubin, F. Bonnier, C. Sandt, L. Venteo, M. Pluot, B. Baehrel, M. Manfait, and G. D. Sockalingum, *Biopolymers*, 2007, **89**, 160–169.
31. F. Bonnier, S. Rubin, L. Debelle, L. Ventéo, M. Pluot, B. Baehrel, M. Manfait, and G. D. Sockalingum, *J. Biophotonics*, 2008, **1**, 204–14.
32. F. Bonnier, D. Bertrand, S. Rubin, L. Ventéo, M. Pluot, B. Baehrel, M. Manfait, and G. D. Sockalingum, *Analyst*, 2008, **133**, 784–90.
33. D. L. Wetzell, L. H. Wetzell, M. D. Wetzell, and R. A. Lodder, *Analyst*, 2009, **134**, 1099–1106.
34. P. A. West, M. P. G. Bostrom, P. A. Torzilli, and N. P. Camacho, *Appl. Spectrosc.*, 2004, **58**, 376–81.
35. S.-S. Kim, C. Young, and B. Mizaiikoff, *Anal. Bioanal. Chem.*, 2008, **390**, 231–7.
36. L. A. Cassis and R. A. Lodder, *Anal. Chem.*, 1993, **65**, 1247–56.

- 1  
2  
3 37.R. J. Dempsey, L. A. Cassis, D. G. Davis, and R. A. Lodder, *Ann. N. Y. Acad. Sci.*, 1997, **820**, 149–69.  
4  
5 38.P. R. Moreno, *Circulation*, 2002, **105**, 923–927.  
6  
7 39.A. Boskey and N. Pleshko Camacho, *Biomaterials*, 2007, **28**, 2465–78.  
8  
9 40.L. Debelle and A. M. Tamburro, *Int. J. Biochem. Cell Biol.*, 1999, **31**, 261–72.  
10  
11 41.R. E. Neuman and M. A. Logan, *J. Biol. Chem.*, 1950, **184**, 299.  
12  
13 42.C. A. Edwards and W. D. O’Brien, *Clin. Chim. Acta*, 1980, **104**, 161–167.  
14  
15 43.R. E. Neuman and M. A. Logan, *J. Biol. Chem.*, 1950, **186**, 549.  
16  
17 44.R.A. Grant, *J. Atheroscler. Res.*, 1967, **7**, 463–472.  
18  
19 45.A. Kohler, C. Kirschner, A. Oust, and H. Martens, *Appl. Spectrosc.*, 2005, **59**, 707–16.  
20  
21 46.P. Bassan, A. Kohler, H. Martens, J. Lee, E. Jackson, N. Lockyer, P. Dumas, M. Brown, N. Clarke,  
22 and P. Gardner, *J. Biophotonics*, 2010, **3**, 609–20.  
23  
24 47.P. Lin, D. A. Reiter, and R. G. Spencer, *J. Magn. Reson.*, 2009, **201**, 61–71.  
25  
26 48.A. Hanifi, X. Bi, X. Yang, B. Kavukcuoglu, P. C. Lin, E. DiCarlo, R. G. Spencer, M. P. G. Bostrom,  
27 and N. Pleshko, *Am. J. Sports Med.*, 2012, **40**, 2853–61.  
28  
29 49.M. V Padalkar, R. G. Spencer, and N. Pleshko, *Ann. Biomed. Eng.*, 2013, **41**, 2426–36.  
30  
31 50.J. M. Rosano, R. Cheheltani, B. Wang, H. Vora, M. F. Kiani, and D. L. Crabbe, *Cardiovasc. Eng.*  
32 *Technol.*, 2012, **3**, 237–247.  
33  
34  
35  
36  
37  
38  
39  
40  
41  
42  
43  
44  
45  
46  
47  
48  
49  
50  
51  
52  
53  
54  
55  
56  
57  
58  
59  
60

1  
2  
3  
4  
5  
6  
7  
8  
9  
10  
11  
12  
13  
14  
15  
16  
17  
18  
19  
20  
21  
22  
23  
24  
25  
26  
27  
28  
29  
30  
31  
32  
33  
34  
35  
36  
37  
38  
39  
40  
41  
42  
43  
44  
45  
46  
47  
48  
49  
50  
51  
52  
53  
54  
55  
56  
57  
58  
59  
60

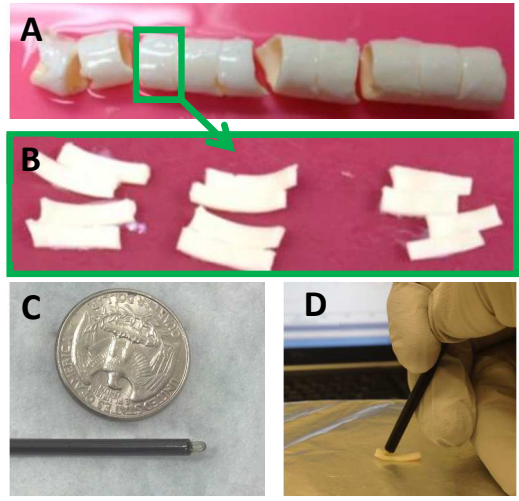


Fig. 1

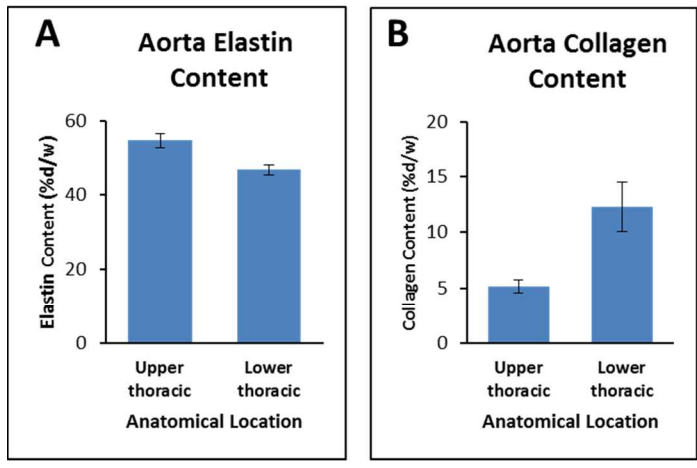


Fig. 2

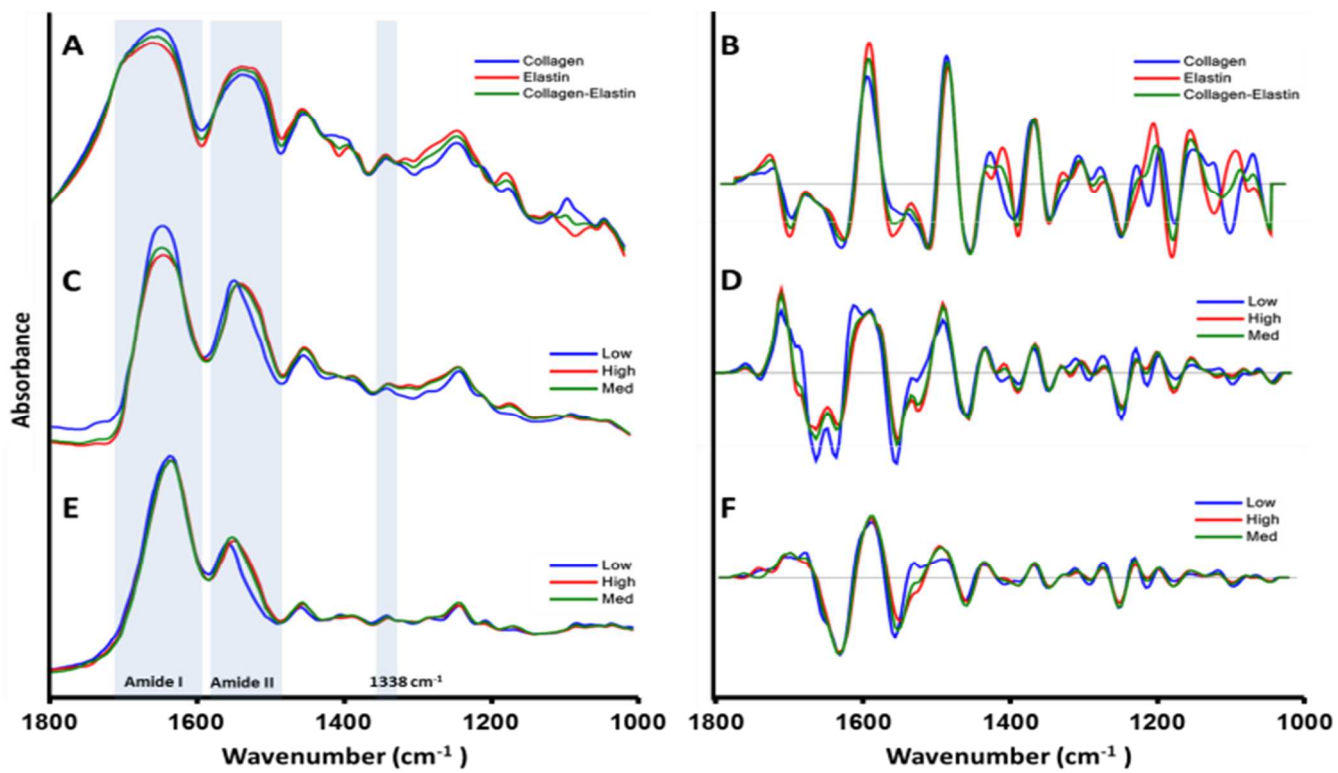


Fig. 3

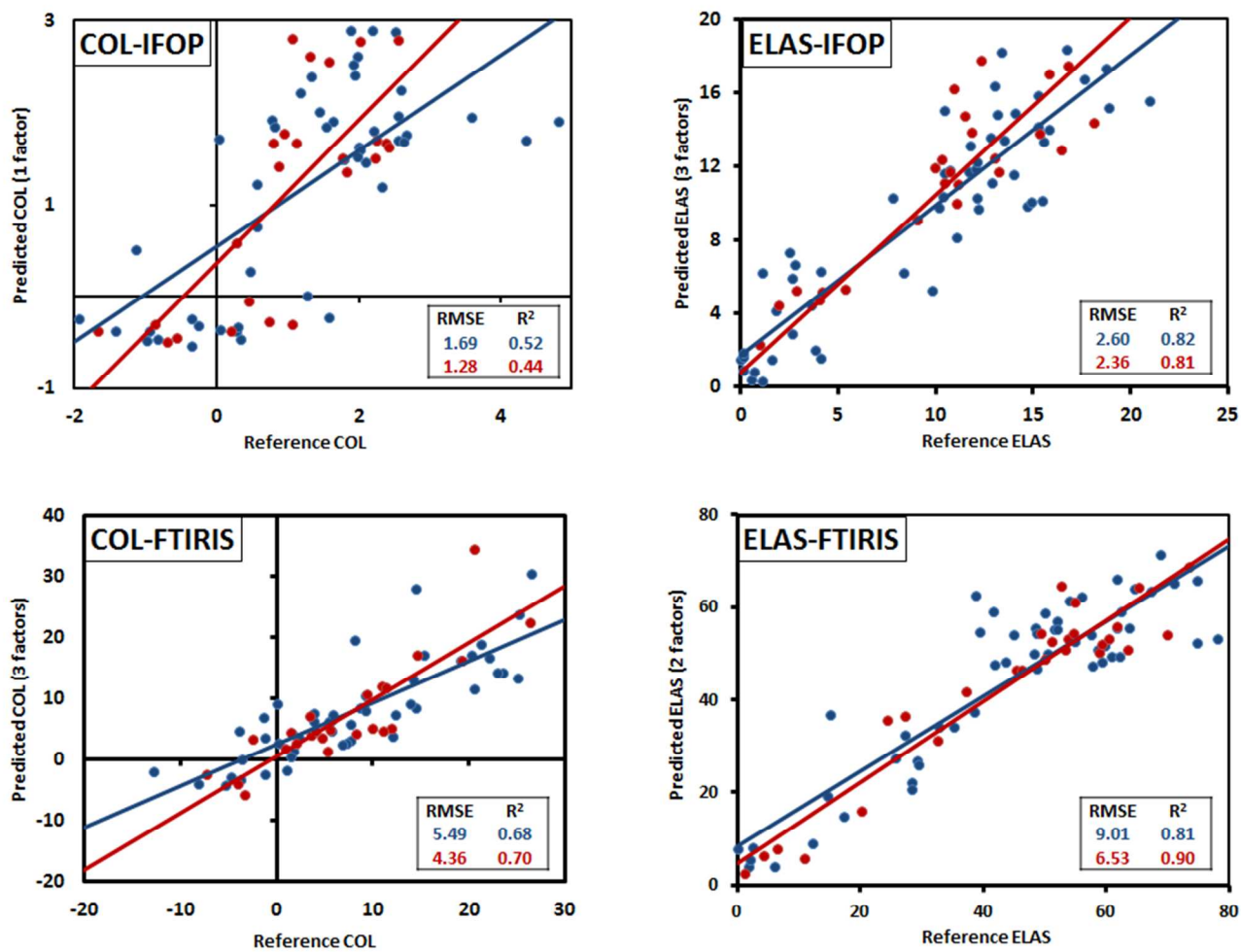


Fig. 4

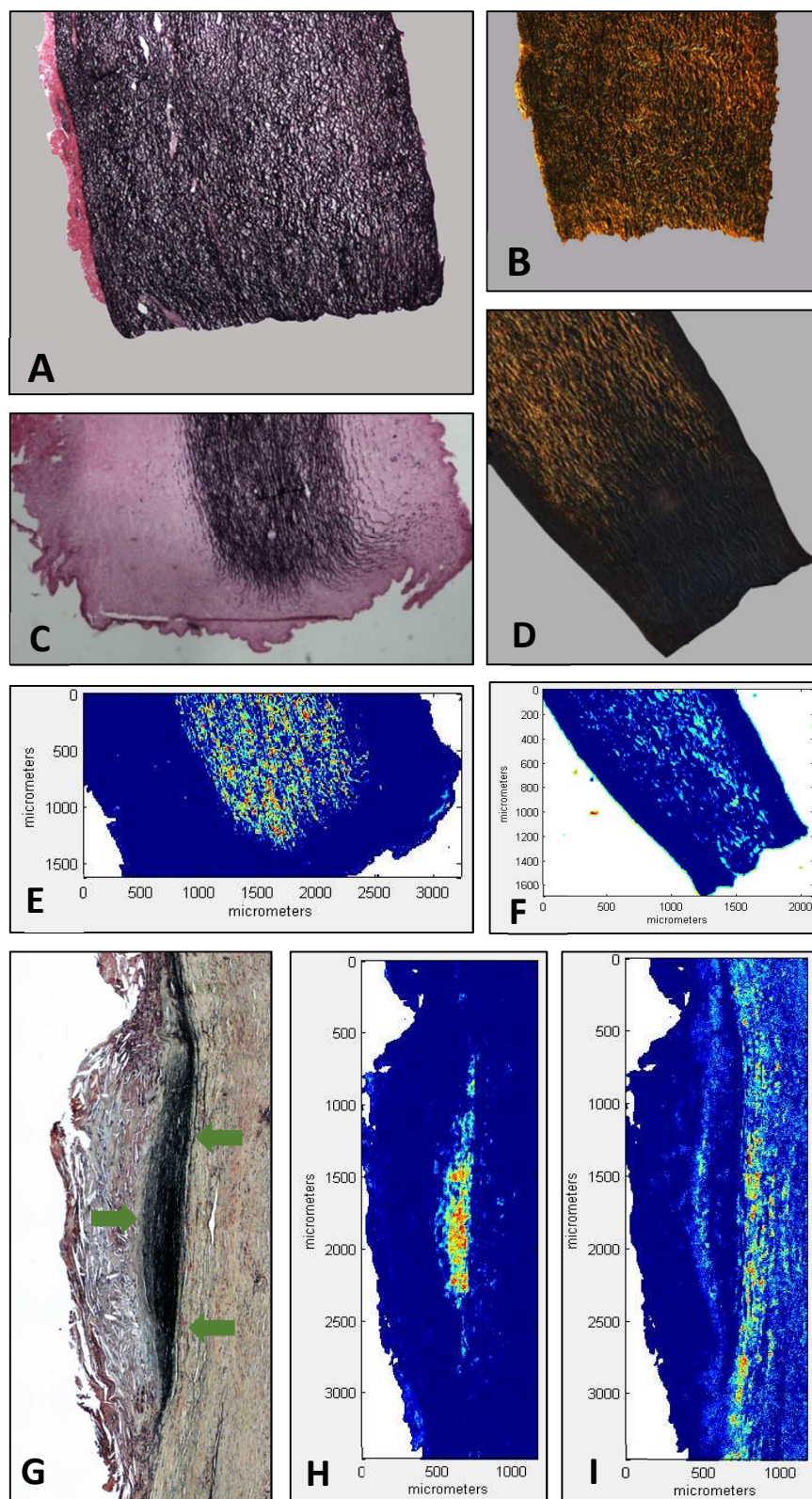


Fig. 5